Proceedings of DETC2010
2010 Proceedings of the ASME 2010 International Design Engineering Technical Conferences & Computers and Information in Engineering Conference
August 15–18, 2010, Montreal Quebec, Canada

DETC2010-28990

A LOW VOLTAGE CONTROLLER FOR A CHAOTIC MICRO RESONATOR

S. Towfighian
Mechanical Engineering
University of Waterloo
Waterloo, ON N2L 3G1, Canada
Email: stowfigh@engmail.uwaterloo.ca

G. R. Heppler
Systems Design Engineering
University of Waterloo
Waterloo, ON N2L 3G1, Canada
Email: heppler@uwaterloo.ca

E. M. Abdel-Rahman*
Systems Design Engineering
University of Waterloo
Waterloo, ON N2L 3G1, Canada
Email: eihab@engmail.uwaterloo.ca

ABSTRACT

The performance of a chaotic micro resonator is improved by redesigning a quadratic controller reported in a previous study. The chaotic micro resonator is composed of an electrostatic actuator and a voltage regulator (controller). The actuator is made of cantilever beam electrode above a fixed electrode. The actuator voltage, and consequently the electrostatic force magnitude, is controlled to drive the cantilever beam oscillations into chaos by creating a bi-stable regime in the system response. The performance of the redesigned controller is improved such that the system input voltage is reduced. The voltage generated by the controller is halved and the controller gains are smaller, which reduces the power and gain demands on the analogue controller components. The static and dynamic responses of the chaotic oscillator are studied and the sizes of the basins of attraction are compared for the improved and the original quadratic controllers. The controller can be configured to create two potential wells. The excitation DC voltages can then be adjusted to control the size of the upper and lower wells and thereby the basins of attraction around the two stable equilibria. As a result, one can shape the chaotic attractor to meet desired criteria. The reported chaos is intermittent chaos located in the lower well and between the two potential wells. This study can be used to design a new generation of nonlinear oscillators targeting high resolution sensors.

*Address all correspondence to this author.

1 Introduction

In contrast to abundant research studies on linear MEMS oscillators, studies on nonlinear oscillators are very limited. Nonlinear oscillators at the macro scale have been successfully developed for health monitoring [1–3] and for detecting corrosion [4]. The sensitivity of the chaotic oscillation was employed to detect very small stiffness changes as small as 15%, in aeroelastic systems [5, 6], and to detect mass variations as small as 0.07% due to corrosion in an aluminum cantilever beam [4]. Such high sensitivities could not be achieved by linear oscillators. Nonlinear chaotic micro-oscillators have not received much attention due to their complex behavior. There are reports of chaotic oscillation in MEMS for atomic force microscopy (AFM) [7–9] and in electrostatic MEMS [10–18], but the target for these studies was to avoid this type of nonlinear vibration. A similar objective was pursued by Park et al. [19] that added a force control to an electrostatic actuator using its displacement feedback and converted the chaotic vibrations to periodic oscillations. In smaller scale NEMS, there are some recent studies on nonlinear vibration, chaos and their applications [20–22]. Bucks et al. [20] found higher mass detection sensitivity is achieved once operating a nanomechanical resonator in the nonlinear region. Conley et al. [21] studied the onset of nonlinear planar motion and nonplanar whirling motion of electrostatically excited nanowires with a proposed application in an overload detection mechanism. The study is then further developed by Chen et al. [22], in which they presented bifurcation diagram for the extensive nonplanar chaotic oscillation of a nanowire at increased AC voltages. Chen et al. [22] suggested applying the chaotic nanowire oscillators in

random number generation used in secure communications.

The focus of this study is to create a chaotic oscillator that shows sustained chaotic oscillation for a wide range of AC and DC excitations that can be used as a nonlinear sensor with higher sensitivity. The chaotic oscillator is comprised of a voltage regulator (controller) added to an electrostatic actuator.

Feedback control in MEMS are reported in a number of studies [18, 19, 23]. Lu et al. [23] used a capacitive sensor for an electrostatic actuator and extended their operation range. The controlled system was then investigated by Liu et. al [18] who reported chaos is the response of the system to strong disturbances. In an extension of their studies, Towfighian et al. [24] presented a comprehensive study of the nonlinear dynamic behavior of the closed loop system and illustrated the bifurcation diagrams for finding the excitation voltage parameters for sustained chaotic oscillations [24]. A new controller to extend the operation ranges of the chaotic oscillation and to decrease the input voltage was designed in a previous study [25]. In this work, the controller has been redesigned to further reduce the input voltage of the system, to reduce the voltage generated by the controller, and to decrease the controller gains and thereby to make it realizable in an analog circuit. In addition, the improved oscillator shows tunability in terms of the location over the gap, which can be useful with regard to different design criterion.

2 System Modeling

The chaotic oscillator system consists of an electrostatic actuator and a voltage regulator(controller). The electrostatic actuator has a cantilever beam above a fixed electrode (Figure 1). Using an Euler-Bernoulli beam model, the equation of motion for a damped cantilever beam in an electrostatic field is a PDE equation:

$$\rho A\frac{\partial^2\hat{w}(\hat{x},\hat{t})}{\partial\hat{t}^2}+EI\frac{\partial^4\hat{w}(\hat{x},\hat{t})}{\partial\hat{x}^4}+c\frac{\partial\hat{w}(\hat{x},\hat{t})}{\partial\hat{t}}=\frac{\varepsilon_0 bV_{DC}^2}{2(d-\hat{w}(\hat{x},\hat{t}))^2} \quad (1)$$

where $\hat{w}(\hat{x},\hat{t})$ is the deflection of the beam in the $\hat{z}$ direction, $\hat{x}$ is the coordinate along the beam length, and $\hat{t}$ is time. The linear viscous damping coefficient per unit length c is used to account for damping losses due to the beam motion through air, A is the cross sectional area, I is the second moment of area, V_{DC} is the applied DC voltage and the other parameters are defined in Table 1.

The equations of motion of the chaotic oscillator containing the electrostatic actuator and the controller then follow where both sides of the electrostatic actuator equation of motion are multiplied by $(d-\hat{w}(\hat{x},\hat{t}))^2$ and then the equations are nondimensionalized:

$$\begin{cases}\ddot{w}(1-w)^2+w^{(4)}(1-w)^2+\mu\dot{w}(1-w)^2=\alpha(V_{in}-\hat{V}_c)^2\\ \dot{\hat{V}}_c=-K_I\big(\hat{V}_c-\dfrac{(a_0+a_1q_1+a_2q_1^2)}{\sqrt{\alpha}}\big)\end{cases} \quad (2)$$

where w is the nondimensional beam deflection (nondimensionalized with respect to the initial gap d) in the $\hat{z}$ direction(Figure 1), which is a function of time and the coordinate along the beam length ($w(x,t)$), q_1 is the nondimensional beam tip deflection, and time t is nondimensional with respect to a time constant

$$T=\sqrt{\frac{\rho AL^4}{EI}}. \quad (3)$$

The two system parameters, μ and α, are given by

$$\mu=2\zeta\omega_n,\ \alpha=\frac{\varepsilon_0 bL^4}{2EId^3} \quad (4)$$

where ζ is the damping ratio found experimentally and ω_n is the nth canonical natural frequency of a cantilever beam. All other parameters used are listed in Table 1. In Equation 2, $\ddot{w}$ and $\dot{w}$ are the second and first derivatives with respect to time and $w^{(4)}$ is the fourth derivative with respect to the coordinate along the length. $\hat{V}_c$ is the output voltage of the controller, and V_{in} is the input voltage consisting of AC and DC components:

$$V_{in}=V_{DC}+V_{AC}\cos(\omega t) \quad (5)$$

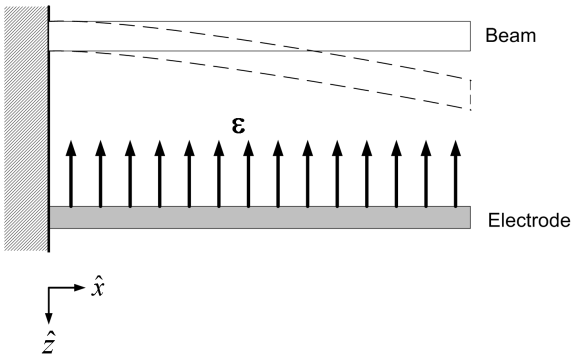

Figure 1: Schematic of the microbeam oscillator (Arrows indicate the field direction).

Table 1: Actuator parameters

Parameter	Symbol	Value
Density	ρ	2331 $\frac{kg}{m^3}$
Beam Length	L	157.4 μm
Beam Width	b	10 μm
Beam height	h	1.9 μm
Initial gap	d	1.9 μm
Nondimensional damping coefficient	μ	0.6153
Permittivity of free space	ε_0	8.85E-12 $\frac{F}{m}$
Modulus of Elasticity	E	150 GPa
Integrator gain	$\frac{K_I}{T}$	0.1776 $\frac{1}{s}$

To obtain the ordinary differential equations of the system, separation of variables is used:

$$w(x,t) = \Phi_1(x)q_1(t) \tag{6}$$

where $\Phi_1(x)$ is the 1st cantilever beam mode shape normalized with respect to the beam tip modal deflection so that $\Phi_1(1) = 1$, and q_1 is the normalized beam tip deflection. Galerkin's method is then applied to obtain a set of ordinary differential equations: (see Towfighian et. al [26] for more details)

$$\begin{cases} (\ddot{q}_1 + \mu\dot{q}_1 + \omega_1^2 q_1)(1 + c_1 q_1 + c_2 q_1^2) = c_3 \alpha (V_{ref} - \hat{V}_c)^2 \\ \dot{\hat{V}}_c = -K_I\big(\hat{V}_c - \dfrac{(a_0 + a_1 q_1 + a_2 q_1^2)}{\sqrt{\alpha}}\big) \end{cases} \tag{7}$$

where c_1, c_2, c_3 are Galerkin's nondimensional coefficients. To implement the electronic circuit of the controller, the second equation is rewritten to include dimensional time:

$$\dot{\hat{V}}_c = -\frac{K_I}{T}\big(\hat{V}_c - \frac{(a_0 + a_1 q_1 + a_2 q_1^2)}{\sqrt{\alpha}}\big) \tag{8}$$

where the value of the integrator gain $\frac{K_I}{T}$ is given in Table 1. The coefficients in the above equation are chosen to be realizable in an electronic circuit and $\hat{V}_c$ has a 35 V range (-15 V to 20 V) as illustrated in Figure 2, which is 2.29 times less voltage compared to the previous design [24].

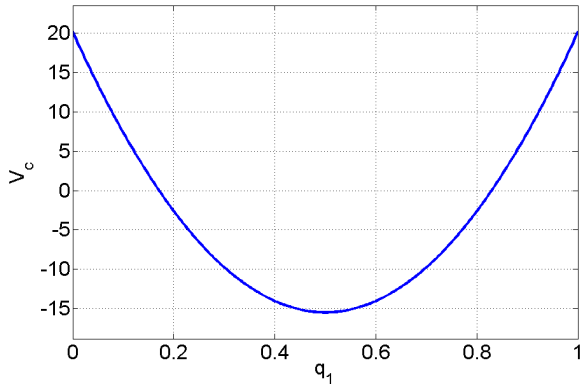

Figure 2: controller output voltage range V_c over the nondimensional gap when controller coefficients are $\frac{a_0}{\sqrt{\alpha}} = 20.1939\ V$, $\frac{a_1}{\sqrt{\alpha}} = 142.6973\ V$, $\frac{a_2}{\sqrt{\alpha}} = 142.6973\ V$.

The parameters for the simulations of the cantilever beam are identified experimentally. The natural frequency of the cantilever beam has been found experimentally to be 99.38 kHz and the beam length was determined to be 157 μm.

3 Static Analysis

The controller is redesigned to generate chaotic vibrations with tunable potential wells and reduced input voltage. To study the behavior of the chaotic actuator, the location of the equilibrium points and their stability conditions should be known. The location of the equilibrium points, the static response, is found from Equation 7 by setting the derivatives to zero, inputing the DC voltage, and solving numerically. The stability of the points are found by linearizing Equation 7 around the equilibrium points and finding the eigenvalues. Static responses for two designs of the controller are illustrated in Figures 3 and 4 and the eigenvalues at $V_{in} = 2$ V in Figure 4 are listed in Table 2.

Table 2: Eigenvalues for the equilibrium points at $V_{in} = 2$ V. (# corresponds to the numbers shown in Figure 4)

#	q_1	Eigenvalue 1	Eigenvalue 2
1	0.066	-0.308+5.72i	-0.308-5.72i
2	0.458	2.43	-3.04
3	0.555	-0.308+2.11i	-0.308-2.11i
4	0.962	15.89	-16.51

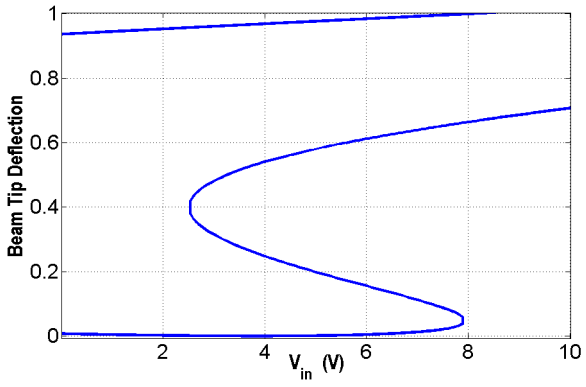

Figure 3: Non-dimensional deflection of the beam tip versus voltage when controller coefficients are $\frac{a_0}{\sqrt{\alpha}} = 3.8697\ V$, $\frac{a_1}{\sqrt{\alpha}} = -88.0195\ V$, $\frac{a_2}{\sqrt{\alpha}} = 104.78\ V$ (first design).

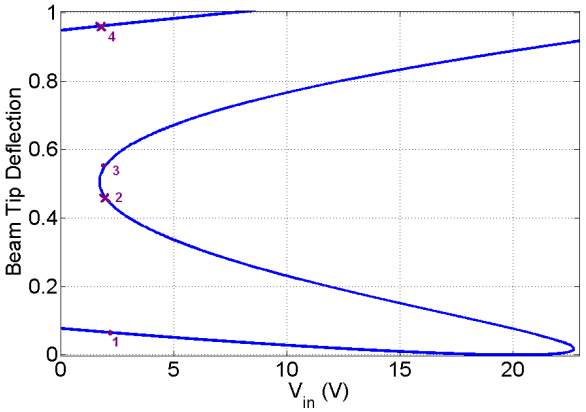

Figure 4: Non-dimensional deflection of the beam tip versus voltage when controller coefficeints are $\frac{a_0}{\sqrt{\alpha}} = 20.1939\ V$, $\frac{a_1}{\sqrt{\alpha}} = 142.6973\ V$, $\frac{a_2}{\sqrt{\alpha}} = 142.6973\ V$ (second design).

It can be concluded from Figure 4, and Table 2 that points 1 and 3 are the stable equilibrium points and points 2 and 4 are unstable eqilibrium points. The nondimensional natural frequency of the lower and upper equilibrium points (1 & 3) are 5.72 and 2.11 and correspond to 161.7 kHz and 59.6 kHz respectively.

The bistability region for the first design in Figure 3 is 5.3 V, which is the same as the bistability range in Towfighian et al. [24], but the bistability range for the second design in Figure 4 is as large as 20.95 V. The first design bi-stability operating voltages are 2.6 V to 7.9 V, whereas the operating votlages for the second desgin are 1.75 V to 22.7 V. The operating voltages show significant reduction in comparison to the 110 V in Towfighian et al. [24] reducing the demand on the electronic components (Figure 5). The first design is suitable when the location of the upper stable equilibrium point is required to be less than 70% of the gap and the input voltage is limited to 8 V. On the other hand, the second design is suitable when the location of the upper eqilibrium point can reach 90% of the gap. The two alternative designs are valuable with regard to different design objectives or potential implementation complications.

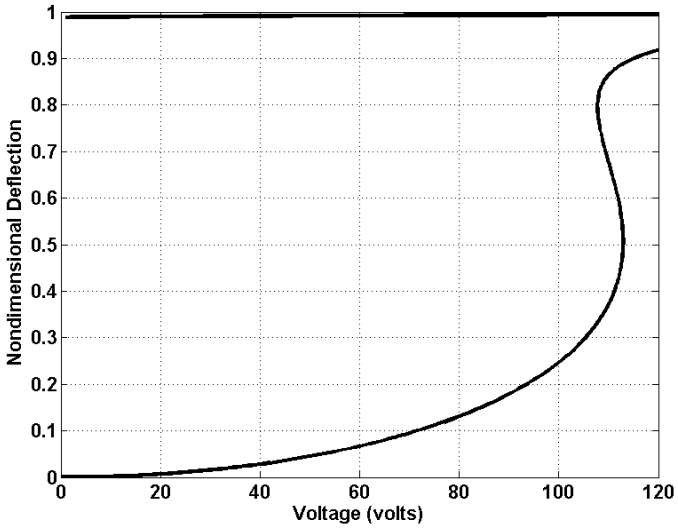

Figure 5: Nondimensional deflection of the beam tip versus voltage V_{DC} for a previous controller design reported in [24].

The redesigned controller has also the advantage of tunability in terms of the size of the potential wells of the chaotic attractor. This property can be seen in Figures 3 and 4. That is, at low voltages in the bistability region, the upper equilibrium point is close to the lower saddle, while the lower equilibrium is farther from the saddle indicating a larger basin of attraction for the lower well. As the voltage increases, it reverses; the upper well basin of attraction becomes larger than the lower well basin.

4 Dynamic Analysis

The steady state dynamic response of the oscillator to AC voltages is found by solving Equations 7 numerically for 5000 periods of AC excitation and keeping the last 128 periods. The DC voltage is set to $V_{DC} = 2$ V and the ranges for AC amplitude and frequency where chaos occurs are found.

Exciting at the nondimensional frequency of 3.2 or the dimensional frequency of 90.4 kHz, which is between the natural frequency of the two equilibrium points, chaos occurs at the AC amplitude of $V_{AC} = 1$ V (Figure 6). Figure 6 shows that the motion develops in the lower well and then it goes beyond the bump and starts oscillating between the two potential wells, then sud-

denly it comes back to the lower well, and the motion repeats itself. This type of chaos is intermittent chaos different from chaos through period doubling [25]. The chaotic motion developed in this case is mostly in the lower well and between the two wells as the phase portrait and times series of the deflection show. The controller voltage is changing between 10 to 19 V and it is significantly reduced from 50 V peak to peak in Towfighian et al [25].

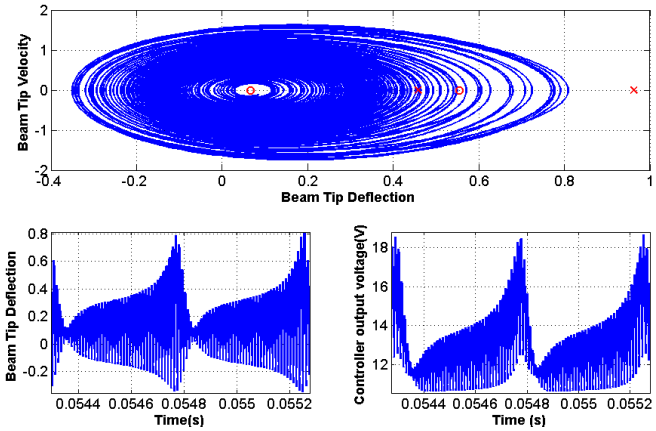

Figure 6: Top: phase portrait of chaotic oscillation , Bottom left: Nondimensioanl beam tip deflection, Bottom right: Controller output voltage V_c, for the second design and $\frac{K_I}{T} = 0.1776\frac{1}{s}$, once DC voltage $V_{DC} = 2$ V, the amplitude of excitation $V_{AC} = 1$ V, and the frequency of excitation is 90.4 kHz. (crosses show the location of saddles and circles show the location of stable equilibrium points)

5 Conclusion

A chaotic oscillator is developed in this study by adding a controller to drive an electrostatic actuator to chaos. The controller has a quadratic function and can be implemented on an analog circuit. It regulates the voltage of the actuator and makes it bi-stable for a range of DC voltage. Controller performance has been improved since a previous study [24] to require less input voltage and to generate half the voltage thus decreasing the electronic circuit component demands.

The static response of the system is presented for two alternative designs of the controller. It reveals that the improved controller not only has a wider voltage range for bistability, but also has lower operating input voltages. The improved controller also offers a chaotic oscillator with tunable basins of attraction. In other words, the expansion of the choatic oscillation over the gap can be adjusted by changing the input DC voltage.

The dynamic steady state response of the system to AC votlages is also presented. By exciting the system with AC voltage at a freqeuncy between the natural frequencies of the two potential wells intermittent chaos is obtained. This intermittent chaotic motion is located in the lower well and between the two potential wells. It is observed that the voltage generated by the controller is significantly reduced since the previous study [25].

Acknowledgment

This research was financially supported by the Natural Sciences and Engineering Research Council of Canada (NSERC) and the Canadian Foundation for Innovation(CFI).

REFERENCES

[1] J.M. Nichols, M.D. Todd, M. Seaver, and L.N. Virgin. Use of chaotic excitation and attractor property analysis in structural health monitoring. *Physical Review E – Statistical*, 67(12):162091–162098, 2003.

[2] B. I. Epureanu, S. H. Yin, and M. M. Derriso. High-sensitivity damage detection based on enhanced nonlinear dynamics. *Smart Materials and Structures*, 14(2):321–327, April 2005.

[3] S. Ghafari. *A Fault Diagnosis System for Rotary Machinary Supported by Rolling Element Bearings*. PhD thesis, University of Waterloo, 2007.

[4] S.-H. Yin and B.I. Epureanu. Experimental enhanced nonlinear dynamics and identification of attractor morphing modes for damage detection. *Journal of Sound and Acoustics*, 129(6):763–770, Dec. 2007.

[5] B. I. Epureanu, L. S. Tang, and M. P. Paidoussis. Exploiting chaotic dynamics for detecting parametric variations in aeroelastic systems. *AIAA Journal*, 42(4):728–735, 2004.

[6] B.I. Epureanu and S.-H. Yin. Identification of damage in an aeroelastic system based on attractor deformations. *Computers & Structures*, 82(31–32):2743–51, Dec. 2004.

[7] M. Basso, L. Giarré, M. Dahleh, and I. Mezic. Numerical analysis of complex dynamics in atomic force microscopes. In *Proceedings of* IEEE *International Conference on control Applications*, pages 1026–1030, Trieste, Italy, Sep. 1998.

[8] M. Ashhab, M.V. Salapaka, M. Dahleh, and I. Mezic. Melnikov-based dynamical analysis of microcantilevers in scanning probe microscopy. *Nonlinear Dynamics*, 20(3):197–220, Nov. 1999.

[9] M. Ashhab, M.V. Salapaka, M. Dahleh, and I. Mezic. Dynamical analysis and control of microcantilevers. *Automatica*, 35(10):1663–1670, Nov. 1999.

[10] J. Bienstman, J. Vandewalle, and R. Puers. Autonomous impact resonator: A new operating principle for a silicon resonant strain gauge. *Sensors and Actuators, A (Physical)*, 66(1-3):40–49, 1998.

[11] Y. C. Wang, S. G. Adams, J. S. Thorp, N. C. MacDonald,

P. Hartwell, and F. Bertsch. Chaos in MEMS, parameter estimation and its potential application. IEEE *Transactions on Circuits and Systems I: Fundamental Theory and Applications*, 45(10):1013–1020, 1998.

[12] B.E. DeMartini, H.E. Butterfield, J. Moehlis, and K.L. Turner. Chaos for a microelectromechanical oscillator governed by the nonlinear mathieu equation. *Journal of Microelectromechanical Systems*, 16(6):1314–1323, Dec. 2007.

[13] Y. Zhang, Y. S. Wang, Z. H. Li, Y. B. Huang, and D. C. Li. Snap-through and pull-in instabilities of an arch-shaped beam under an electrostatic loading. *Journal of Microelectromechanical Systems*, 16(3):684–693, 2007.

[14] S. Krylov. Lyapunov exponents as a criterion for the dynamic pull-in instability of electrostatically actuated microstructures. *International Journal of Non-Linear Mechanics*, 42(4, pp. 626-642):May, 2007.

[15] S. Krylov, B. R. Ilic, D. Schreiber, S. Seretensky, and H. Craighead. The pull-in behavior of electrostatically actuated bistable microstructures. *Journal of Micromechanics and Microengineering*, 18(5):1–20, May 2008.

[16] K. Das and R. C. Batra. Pull-in and snap-through instabilities in transient deformations of microelectromechanical systems. *Journal of Micromechanics and Microengineering*, 19(3), 20090101 2009.

[17] Jeffrey F. Rhoads, Steven W. Shaw, Jeff Moehlis, Barry E. Demartini, Kimberly L. Turner, and Wenhua Zhang. Nonlinear response of parametrically-excited mems. In *DETC2005: ASME International Design Engineering Technical Conferences and Computers and Information in Engineering Conference*, volume 1 A, pages 453–461, 2005.

[18] S. Liu, A. Davidson, and Q. Lin. Simulation studies on nonlinear dynamics and chaos in a MEMS cantilever control system. *Journal of Micromechanics and Microengineering*, 14(7):1064–1073, 2004.

[19] K. Park, Q. Chen, and Y.C. Lai. Energy enhancement and chaos control in microelectromechanical systems. *Physical Review E 77*, 77:026210–1–6, 2008.

[20] E. Buks and B. Yurke. Mass detection with a nonlinear nanomechanical resonator. *Physical Review E*, 74(4):46619–461–9, Oct. 2006.

[21] W.G. Conley, A. Raman, C. M. Krousgrill, and S. Mohammadi. Nonlinear and nonplanar dynamics of suspended nanotube and nanowire resonators. *Nano Letters*, 8(6):1590–1595, 2008.

[22] Q. Chen, L. Huang, Y. C. Lai, C. Grebogi, and D. Dietz. Extensively chaotic motion in electrostatically driven nanowires and applications. *Nano letters*, 10(2):406–413, Feb. 2010.

[23] M. S.-C. Lu and G. K. Fedder. Position control of parallel-plate microactuators for probe-based data storage. *Journal of Microelectromechanical Systems*, 13(5):759–769, Oct. 2004.

[24] S. Towfighian, G. R. Heppler, and E. M. Abdel-Rahman. Analysis of a chaotic electrostatic micro-oscillator. *Journal of Computational and Nonlinear Dynamics*, In press, Accepted in Feb. 2010.

[25] S. Towfighian, G. R. Heppler, and E. M. Abdel-Rahman. Quadratic controller for a chaotic micro-resonator. In *Proceedings of 2nd Microsystems and Nanoelectronics Research Conference*, pages 69–72, Ottawa, Canada, 2009.

[26] S. Towfighian, E. M. Abdel-Rahman, and G. R. Heppler. Static and dynamic analysis of a bistable micro-actuator. In *Proceedings of ASME International Mechanical Engineering Congress and Exposition*, pages 1–11, Boston, MA, USA, 2008.